14th International Symposium on Turbulence and Shear Flow Phenomena (TSFP14)
Heidelberg, Germany, July 28–31, 2026

DIRECT NUMERICAL SIMULATION OF THE COMPRESSIBLE TURBULENT BOUNDARY LAYER OVER A ROD-ROUGHENED WALL

Youtian Su
Department of Engineering Mechanics
Tsinghua University
Beijing 100084, PR China
syt22@mails.tsinghua.edu.cn

Weixi Huang
Department of Engineering Mechanics
Tsinghua University
Beijing 100084, PR China
hwx@tsinghua.edu.cn

Chunxiao Xu
Department of Engineering Mechanics
Tsinghua University
Beijing 100084, PR China
xucx@tsinghua.edu.cn

ABSTRACT

Direct numerical simulations (DNS) are performed to investigate the combined effects of surface roughness and wall heat transfer on spatially developing compressible turbulent boundary layers (CTBL) at $Ma = 2.5$. The roughness consists of transverse square bars with $\lambda_x/k = 8$ and $k^+ \approx 35$. Dynamically, a fitting-based optimization procedure is proposed to determine the kinematic virtual origin, successfully restoring the logarithmic behavior. Based on this displacement, Griffin–Fu–Moin (GFM) transformation outperforms the classical van Driest transformation in recovering outer-layer similarity. Thermodynamically, the physical disparity between momentum form drag and the absence of a corresponding heat transfer mechanism disrupts the classical Reynolds analogy. The effective turbulent Prandtl number (Pr_e) deviates severely from unity within the roughness sublayer, leading to the breakdown of the classical Generalized Reynolds Analogy (GRA). To address this, a modified rough-wall GRA (rGRA) is formulated by introducing an equivalent slip-plane, which accurately reconstructs the temperature-velocity relationship by bypassing near-wall thermal heterogeneity.

INTRODUCTION

Compressible wall-bounded turbulent flows are governed by complex kinematic and thermodynamic characteristics. For smooth walls, mean velocity and temperature profiles are well-described by transformations such as van Driest (Van Driest, 1951) and GFM (Griffin et al., 2021), alongside the Generalized Reynolds Analogy (GRA) (Zhang et al., 2014). However, surface roughness fundamentally alters near-wall coherent structures and transport mechanisms, posing severe challenges to these smooth-wall-based models.

In dynamics, the study of rough-wall turbulence centers on outer-layer similarity hypothesis. While compressibility transformations aim to recover this similarity, two-dimensional (2D) roughness—comprising transverse square bars—induces intense flow separation and complex wake interference. Such perturbations extend significantly into the boundary layer. Thermodynamically, the physical asymmetry between pressure drag and heat conduction disrupts the similarity between momentum and heat transport (Dipprey & Sabersky, 1963). Recent studies (Cogo et al., 2025a,b) have demonstrated that while the GRA provides reasonable predictions in the outer layer, systematic deviations persist within the roughness sublayer near the elements. These observations suggest that intensified roughness effects violate the underlying smooth-wall assumptions, such as the spatial homogeneity and constant effective turbulent Prandtl number. Consequently, new theoretical frameworks are required to map the thermodynamic behavior of compressible rough-wall turbulence back to universal profiles.

METHODOLOGY

The computational framework utilizes a dual-domain strategy, as schematically illustrated in figure 1: an auxiliary domain simulating a compressible equivalent boundary layer (CEBL) to generate realistic inflow turbulence (Li et al., 2024), and a main domain for the spatially developing compressible turbulent boundary layer (CTBL). The simulations operate at a freestream Mach number of $M_\infty = 2.5$, investigating combinations of smooth and rough walls under adiabatic ($T_w/T_r = 1.0$) and cold-wall ($T_w/T_r = 0.5$) conditions.

The main CTBL domain solves the standard three-dimensional compressible Navier–Stokes equations. The auxiliary CEBL domain introduces specific source terms to these equations, applying periodic boundary conditions to efficiently generate fully developed turbulence (Li et al., 2024). For rough-wall cases, the surface geometry is modeled as two-dimensional spanwise square bars with a height of $k \approx 0.08\delta_{in}$ and a streamwise pitch of $\lambda_x = 8k$, consistent with canonical configurations (Lee & Sung, 2007; Lee et al., 2011). The four designated simulation cases consist of the smooth-wall configurations (M2p5SA and M2p5SC) with a target friction Reynolds number of $Re_\tau = 510$, and the rough-wall configurations (M2p5RA and M2p5RC) targeting $Re_\tau = 1050$, where the suffixes 'A' and 'C' denote adiabatic and cold-wall conditions, respectively.

The simulations are performed using the high-fidelity finite-difference solver OpenCFD (Li et al., 2010). The complex rough-wall geometry is resolved using a sharp-interface ghost-cell immersed boundary method (IBM) (De Vanna et al., 2020) on a structured Cartesian mesh.

MEAN VELOCITY TRANSFORMATIONS

To accurately determine the zero-plane displacement and recover a standard logarithmic region, a rigorous mathematical optimization procedure is proposed, formulated as follows:

$$\mathscr{Y}^{\oplus} \equiv \ln\left(y^{\oplus} - d^{\oplus}\right), \tag{1a}$$

$$\mathscr{I}(d^{\oplus}) = \left\{ \mathscr{Y}^{\oplus} : \left| \frac{\mathrm{d}u^{\oplus}}{\mathrm{d}\mathscr{Y}^{\oplus}} - \frac{1}{\kappa} \right| \leqslant \frac{0.1}{\kappa} \right\} = \bigcup_{i \in I} [a_i, b_i], \tag{1b}$$

$$F(d^{\oplus}) \equiv \max_{i \in I} (b_i - a_i), \tag{1c}$$

$$d^{\oplus}_{\mathrm{opt}} = \underset{d^{\oplus}}{\mathrm{argmax}} F(d^{\oplus}). \tag{1d}$$

Here, $d^{\oplus}$ represents the trial zero-plane displacement in the inner-scaled coordinate under velocity transformations. The optimization process first defines a modified logarithmic coordinate $\mathscr{Y}^{\oplus}$ (1a) and identifies continuous intervals $\mathscr{I}(d^{\oplus})$ (1b) where the velocity derivative strictly falls within a $\pm 10\%$ tolerance band of the theoretical inverse von Kármán constant ($1/\kappa$). An objective function $F(d^{\oplus})$ (1c) evaluates the maximum continuous length of these valid logarithmic regions. Finally, the optimal zero-plane displacement $d^{\oplus}_{\mathrm{opt}}$ is obtained by globally maximizing this objective function (1d). Utilizing this kinematic optimization, the derived dimensionless zero-plane heights differ significantly from the classical zero-moment estimates. Specifically, under the classical inner scaling (d^+/k^+) and the GFM inner scaling (d^*/k^*), the values are 0.23 and 0.15 for the adiabatic rough-wall case (M2p5RA), and 0.30 and 0.21 for the cold rough-wall case (M2p5RC), respectively. A stark contrast is observed between the kinematically optimized zero-plane displacements and the estimates derived from the classical zero-moment method (Jackson, 1981), which yield significantly higher values of $d_m/k = 0.60$ and 0.64 for the adiabatic and cold-wall cases, respectively.

Utilizing the mathematically optimized zero-plane displacements, the mean velocity profiles are evaluated to assess the roughness function ΔU^+ and outer-layer similarity. When scaled by the van Driest (VD) transformation (Figure 2a), the freestream velocity difference between the adiabatic and cold-wall rough cases remains marginal. While the cold wall exhibits a higher logarithmic intercept (resulting in a smaller ΔU^+), the wake region velocity increases more rapidly for the adiabatic case. Notably, as shown in the outer-scaled velocity defect profiles (Figure 2b), substantial discrepancies exist among the profiles, explicitly indicating an absence of outer-layer similarity under the VD framework.

Conversely, applying the generalized velocity transformation (GFM) yields a significantly more unified scaling (Figure 3a). Under the GFM framework, the difference in the roughness function ΔU^+ between the thermal conditions becomes more pronounced. Compared to the incompressible baseline of $\Delta U^+ = 9.86$ established by Lee & Sung (2007), the adiabatic ΔU^+ values are consistently higher (~ 10.8), whereas the cold-wall case yields a slightly lower $\Delta U^+ = 9.5$. Upon correcting for this velocity deficit, the adiabatic rough-wall profile exhibits an excellent collapse with the reference compressible data of Pirozzoli & Bernardini (2011) ($Ma = 2.0$, $Re_\tau = 1000$) in the region strictly above the roughness crest, maintaining reasonable agreement in the outer wake region. Furthermore, the shape of the wake-region deviation from the universal log-law is remarkably consistent between the two thermal conditions.

The recovery of outer-layer similarity is unequivocally demonstrated by the GFM velocity defect profiles in Figure 3b. All four $Ma = 2.5$ cases—encompassing both smooth and rough walls under adiabatic and cold-wall conditions—exhibit a satisfactory collapse in the region of $y^o > 0.4$. This confirms that for a given freestream Mach number, the GFM transformation successfully maps the wake profile of a rough wall to a shape consistent with the smooth-wall baseline, regardless of wall heat transfer. Discernible differences remain when comparing the present $Ma = 2.5$ series with the $Ma = 2.0$ data of Pirozzoli & Bernardini (2011), which shows a minor departure for $y^o < 0.6$. This indicates that while the transformation accounts for thermal effects, the inherent shape of the wake region still varies with the freestream Mach number.

GENERALIZED REYNOLDS ANALOGY

For smooth boundary layers, the mean temperature field is reliably reconstructed using the classical generalized Reynolds analogy (GRA) (Zhang et al., 2014).

$$\begin{aligned} \frac{\bar{T}}{\bar{T}_\delta} =& \frac{\bar{T}_w}{\bar{T}_\delta} + \left(\frac{\bar{u}_\delta}{\bar{T}_\delta}\Gamma_w\right)\left(\frac{\bar{u}}{\bar{u}_\delta}\right) \\ &+ \left(\frac{\bar{T}_\delta - \bar{T}_w}{\bar{T}_\delta} - \frac{\bar{u}_\delta}{\bar{T}_\delta}\Gamma_w\right)\left(\frac{\bar{u}}{\bar{u}_\delta}\right)^2 \end{aligned} \tag{2}$$

However, this framework exhibits significant limitations for compressible rough-wall boundary layers, particularly under cold-wall conditions (Figure 4). The classical GRA relies on the ratio of actual wall heat flux to skin friction. Yet, the flow beneath the roughness crest exhibits an abrupt thermal shift with only marginal velocity variations, rendering this boundary constraint fundamentally inadequate.

To accurately reconstruct the temperature profiles, the formulation must bypass the highly heterogeneous roughness sublayer. We establish a reference-point method, introducing dynamic and thermal information from an arbitrary outer-region point as a physical constraint. This approach is strictly mathematically equivalent to integrating from a postulated virtual slip-wall. Evaluating the differential relation at an arbitrary reference point i and another outer-region point j yields:

$$\bar{T}_i - \bar{T}_w = \frac{\bar{u}_i - u_w}{2}\left[\Gamma_w + \left.\frac{\partial \bar{T}}{\partial \bar{u}}\right|_i\right] \tag{3a}$$

$$\bar{T}_j - \bar{T}_w = \frac{\bar{u}_j - u_w}{2}\left[\Gamma_w + \left.\frac{\partial \bar{T}}{\partial \bar{u}}\right|_j\right] \tag{3b}$$

Subtracting these equations directly eliminates the virtual wall parameters, leading to:

$$\bar{T}_j - \bar{T}_i = \frac{\bar{u}_j - \bar{u}_i}{2}\left[\left.\frac{\partial \bar{T}}{\partial \bar{u}}\right|_i + \left.\frac{\partial \bar{T}}{\partial \bar{u}}\right|_j\right] \tag{4}$$

Consequently, for any selected reference height h, the modified rough-wall generalized Reynolds analogy (rGRA) is strictly formulated as:

$$\begin{aligned}\bar{T}_{\mathrm{rGRA}}(h,\bar{u}) =& \bar{T}_h + \left(\left.\frac{\partial \bar{T}}{\partial \bar{u}}\right|_h\right)(\bar{u} - u_h) \\ &+ \left(\bar{T}_\delta - \bar{T}_h - (\bar{u}_\delta - u_h)\left.\frac{\partial \bar{T}}{\partial \bar{u}}\right|_h\right)\left(\frac{\bar{u} - u_h}{\bar{u}_\delta - u_h}\right)^2\end{aligned} \tag{5}$$

The physical necessity of selecting an appropriate reference height is elucidated by examining the spatial distributions of the time-averaged temperature (Figure 5). The failure of the classical GRA and the varying accuracy of the rGRA stem directly from the disparate spatial recovery rates of the dynamic and thermal fields. While the velocity field recovers to a wall-parallel state relatively quickly above the roughness elements, the thermal field over a rough surface subjected to substantial heat transfer requires a significantly larger wall-normal distance to achieve spatial homogeneity. For the adiabatic case (Figure 5), the thermal heterogeneity is mild; thus, rGRA profiles anchored at k, $2k$, and $3k$ all exhibit excellent agreement with DNS data (Figure 4a). Conversely, for the cold-wall case (Figure 5), intense thermal heterogeneity extends well above the crest. Consequently, the rGRA anchored precisely at the crest ($h = k$) still exhibits notable discrepancies. However, as the reference height is elevated to $2k$ and $3k$, it effectively bypasses this highly heterogeneous thermal layer, allowing the rGRA to completely recover its accuracy and provide a highly precise description of the outer-region temperature-velocity relationship (Figure 4b).

CONCLUSIONS

DNS of spatially developing CTBL at $Ma = 2.5$ over two-dimensional (2D) roughness reveals that traditional zero-moment methods are inherently inadequate for 2D cavity-type roughness; instead, a fitting-based optimization procedure is shown to be necessary to objectively restore the logarithmic law. Regarding the mean field, the GFM transformation is found to effectively preserve outer-layer similarity, even under non-adiabatic conditions. Furthermore, the intrinsic physical asymmetry between pressure drag and heat transfer is shown to disrupt the classical GRA framework. In contrast, the proposed rGRA, which bypasses the strong near-wall heterogeneity, accurately reconstructs the mean temperature field across both adiabatic and cold-wall conditions.

ACKNOWLEDGEMENTS

This work was supported by National Natural Science Foundation of China (Grant Nos. U2570214, 12425206 and 12388101).

REFERENCES

Cogo, Michele, Modesti, Davide, Bernardini, Matteo & Picano, Francesco 2025a Surface roughness effects on subsonic and supersonic turbulent boundary layers. Journal of Fluid Mechanics 1009, A56.

Cogo, Michele, Modesti, Davide, Picano, Francesco & Bernardini, Matteo 2025b Development of supersonic turbulent boundary layers over prism-shaped rough surfaces. Journal of Fluid Mechanics 1025, A21.

De Vanna, Francesco, Picano, Francesco & Benini, Ernesto 2020 A sharp-interface immersed boundary method for moving objects in compressible viscous flows. Computers & Fluids 201, 104415.

Dipprey, Duane F & Sabersky, Rolf H 1963 Heat and momentum transfer in smooth and rough tubes at various prandtl numbers. International Journal of Heat and Mass Transfer 6 (5), 329–353.

Griffin, Kevin Patrick, Fu, Lin & Moin, Parviz 2021 Velocity transformation for compressible wall-bounded turbulent flows with and without heat transfer. Proceedings of the National Academy of Sciences 118 (34), e2111144118.

Jackson, PS 1981 On the displacement height in the logarithmic velocity profile. Journal of fluid mechanics 111, 15–25.

Lee, Jae Hwa, Sung, Hyung Jin & Krogstad, Per-Åge 2011 Direct numerical simulation of the turbulent boundary layer over a cube-roughened wall. Journal of Fluid Mechanics 669, 397–431.

Lee, Seung-Hyun & Sung, Hyung Jin 2007 Direct numerical simulation of the turbulent boundary layer over a rod-roughened wall. Journal of Fluid Mechanics 584, 125–146.

Li, Rui-Xin, Huang, Wei-Xi & Xu, Chun-Xiao 2024 Inflow turbulence generation for compressible turbulent boundary layers. Physics of Fluids 36 (2).

Li, Xin-Liang, Fu, De-Xun, Ma, Yan-Wen & Liang, Xian 2010 Direct numerical simulation of compressible turbulent flows. Acta Mechanica Sinica 26 (6), 795–806.

Pirozzoli, Sergio & Bernardini, Matteo 2011 Turbulence in supersonic boundary layers at moderate reynolds number. Journal of Fluid Mechanics 688, 120–168.

Van Driest, Edward R 1951 Turbulent boundary layer in compressible fluids. Journal of the Aeronautical Sciences 18 (3), 145–160.

Zhang, You-Sheng, Bi, Wei-Tao, Hussain, Fazle & She, Zhen-Su 2014 A generalized reynolds analogy for compressible wall-bounded turbulent flows. Journal of Fluid Mechanics 739, 392–420.

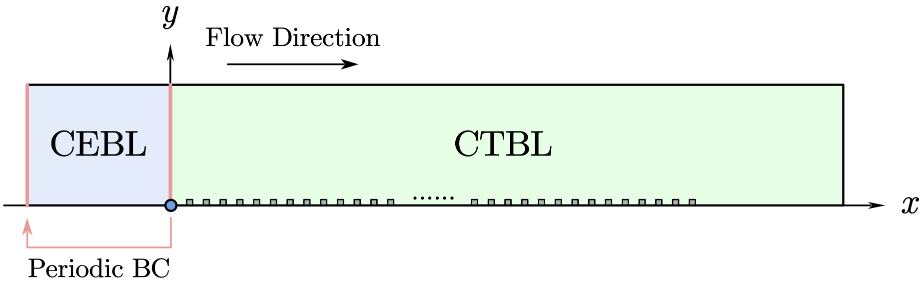

Figure 1: Schematic of the computational domain configurations, comprising the upstream compressible equivalent boundary layer (CEBL) domain and the downstream main compressible turbulent boundary layer (CTBL) domain. The blue dot indicates the origin of the coordinate system, with the streamwise direction aligned with the positive x-axis.

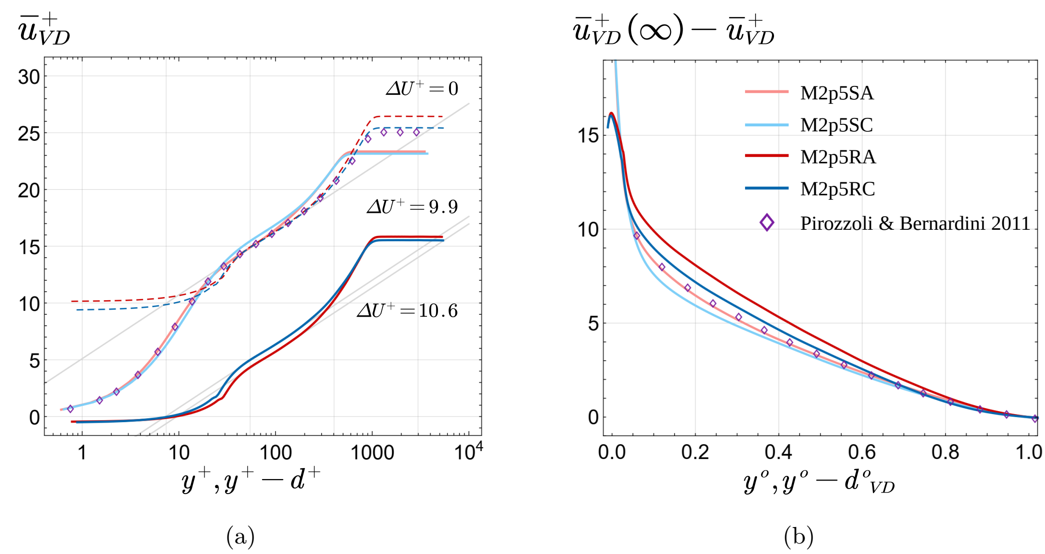

Figure 2: Van Driest (VD) transformation analysis: (a) Inner-scaled mean streamwise velocity profiles; (b) Velocity defect profiles.

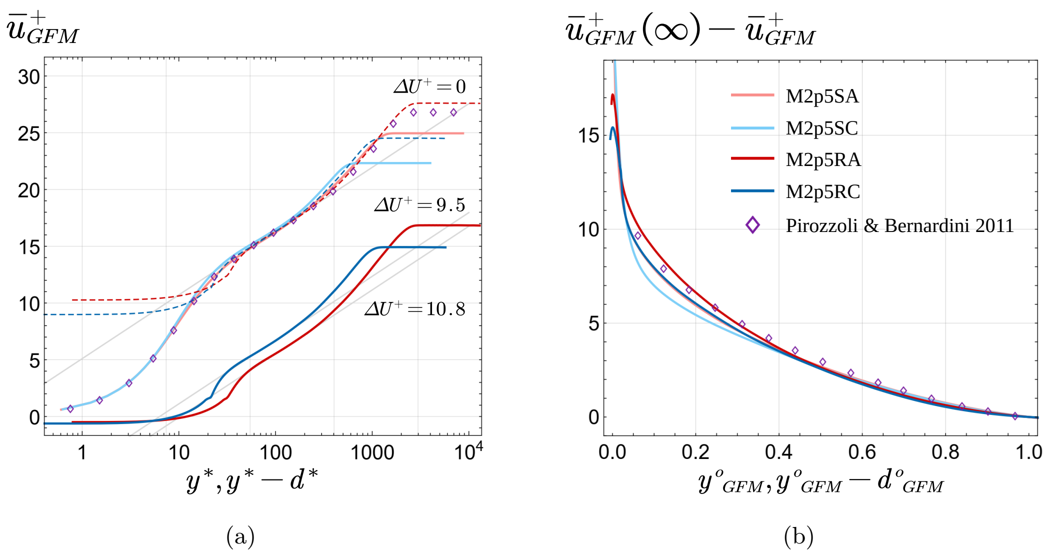

Figure 3: GFM transformation analysis: (a) Inner-scaled mean streamwise velocity profiles; (b) Velocity defect profiles.

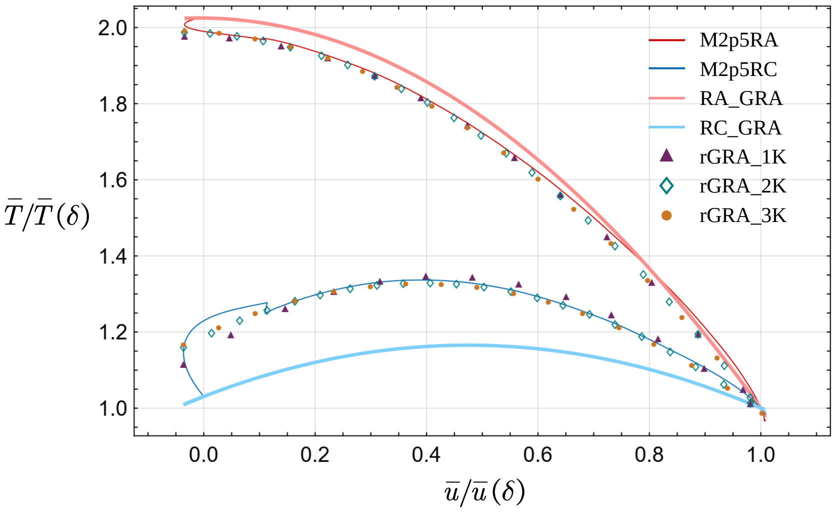

Figure 4: Comparison of velocity-temperature relationships for adiabatic and cold-wall cases. The classical GRA is evaluated using the actual wall heat flux and skin friction, while the rGRA is anchored at three reference heights: $h = k$, $2k$, and $3k$.

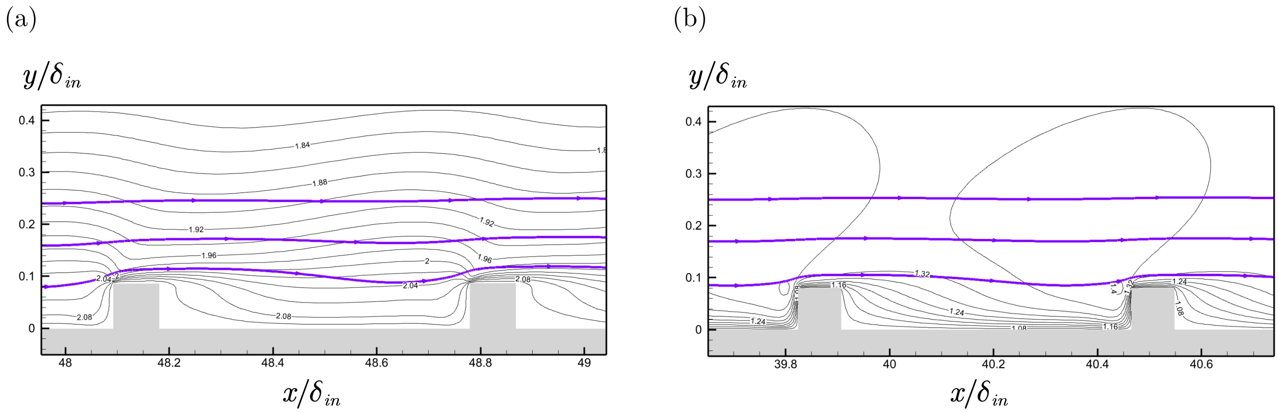

Figure 5: Spatial distributions of the time-averaged temperature. (a) Adiabatic rough-wall case (M2p5RA); (b) cold rough-wall case (M2p5RC). Purple lines represent streamlines in the vicinity of the roughness heights k, $2k$, and $3k$.